NeuroImage **12,** 230–239 (2000)
doi:10.1006/nimg.2000.0599, available online at http://www.idealibrary.com on IDEAL®

A Method for Removing Imaging Artifact from Continuous EEG Recorded during Functional MRI

Philip J. Allen,* Oliver Josephs,† and Robert Turner†

*Department of Clinical Neurophysiology, National Hospital for Neurology and Neurosurgery, University College London Hospitals, Queen Square, London WC1N 3BG, United Kingdom; and †The Wellcome Department of Cognitive Neurology, Institute of Neurology, University College London, Queen Square, London, United Kingdom

Received December 2, 1999

Combined EEG/fMRI recording has been used to localize the generators of EEG events and to identify subject state in cognitive studies and is of increasing interest. However, the large EEG artifacts induced during fMRI have precluded simultaneous EEG and fMRI recording, restricting study design. Removing this artifact is difficult, as it normally exceeds EEG significantly and contains components in the EEG frequency range. We have developed a recording system and an artifact reduction method that reduce this artifact effectively. The recording system has large dynamic range to capture both low-amplitude EEG and large imaging artifact without distortion (resolution 2 μV, range 33.3 mV), 5-kHz sampling, and low-pass filtering prior to the main gain stage. Imaging artifact is reduced by subtracting an averaged artifact waveform, followed by adaptive noise cancellation to reduce any residual artifact. This method was validated in recordings from five subjects using periodic and continuous fMRI sequences. Spectral analysis revealed differences of only 10 to 18% between EEG recorded in the scanner without fMRI and the corrected EEG. Ninety-nine percent of spike waves (median 74 μV) added to the recordings were identified in the corrected EEG compared to 12% in the uncorrected EEG. The median noise after artifact reduction was 8 μV. All these measures indicate that most of the artifact was removed, with minimal EEG distortion. Using this recording system and artifact reduction method, we have demonstrated that simultaneous EEG/fMRI studies are for the first time possible, extending the scope of EEG/fMRI studies considerably.

INTRODUCTION

Combined electroencephalogram (EEG) and functional MRI (fMRI) recording has been used to localize areas of increased blood flow associated with specific EEG events. This has found application in epilepsy (Warach *et al.,* 1996; Krakow *et al.,* 1999; Seeck *et al.,* 1998), α rhythm (Patel *et al.,* 1997), and sleep (Huang-Hellinger *et al.,* 1995). EEG can also be used to assess subject state in cognitive fMRI studies (Portas *et al.,* 1999). High-quality EEG recording is crucial to these studies. EEG quality in the MR scanner is compromised by artifacts caused by interaction between the subject, EEG electrode assemblies, and the scanner's magnetic fields (Allen *et al.,* 1998). The three most significant causes of EEG artifacts in the scanner are (1) gross movements in the static (B_0) field, for example swallowing; (2) the cardioballistogram and blood flow effects in the B_0 field associated with the subject's pulse; and (3) the changing fields applied during fMRI image acquisition. Gross movement causes large artifacts (Hill *et al.,* 1995) but these are normally infrequent. Pulse artifact is potentially a significant problem as it is normally large amplitude, widespread on the scalp, and continuous (that is, occurring even when images are not being acquired). A method for reducing this artifact to acceptable levels has been published (Allen *et al.,* 1998) and this appears to perform reliably (we have now used this method to successfully record over 120 spike-triggered EEG/fMRI studies).

FMRI is normally performed using echo-planar imaging with blood oxygenation level-dependent (BOLD) contrast. Artifacts induced by this imaging technique are normally very large and obscure the EEG completely. For this reason most EEG/fMRI studies have used aperiodic fMRI, i.e., image acquisition triggered immediately after observation of the EEG event of interest. This has two disadvantages. First, EEG events during image acquisition may be missed and confound results—this dictates that each imaging period must be as short as possible, reducing study flexibility. Second, aperiodic fMRI requires a long refractory period after image acquisition to allow complete T1 relaxation, which lengthens study time. Spike-triggered fMRI studies last typically over 1 h (Krakow *et al.,* 1999), so reducing study time would have important benefits for increasing the general application of the technique and reducing the likelihood of subject

1053-8119/00 $35.00

movement. Imaging artifact is also a significant problem for EEG/fMRI sleep studies, as obscured sections of EEG compromise the reliability of sleep staging. In addition, elimination of imaging artifact would allow detection of EEG events during periodic or continuous fMRI. This would desynchronize BOLD signal sampling and EEG events, allowing optimal investigation of the BOLD signal time course (Josephs *et al.*, 1997). It would also allow a subject's state of attention to be monitored during cognitive studies, assisting the interpretation of these studies. Clearly, a method to remove imaging artifact would extend significantly the scope and power of EEG/fMRI studies.

Several techniques for reducing imaging artifact have been reported. Simply applying low-pass filtering is unlikely to be effective as the electromotive forces (emfs) induced by the gradient fields contain energy in the EEG frequency band (0.5–70 Hz). Felblinger has shown that fourth-order low-pass filtering with a cutoff point as low as 13 Hz cannot suppress imaging artifact in ECG signals and gives considerable ECG signal distortion (Felblinger *et al.*, 1999). In this context, EEG and ECG signals have similar spectral content so similar results would be expected for EEG. Kreger described a method for reducing imaging artifact in ECG signals based on adaptive noise cancellation (ANC) (Kreger and Giordano, 1992). The *x*, *y*, and *z* gradient waveforms derived from the scanner were processed with a filter which matched the ECG filter and these formed the reference signals for the ANC algorithm. No quantitative results were given and its applicability to EEG during fMRI is unknown. Laudon used an external loop placed over ECG electrodes to record the induced emf and then subtracted this electronically from the ECG signal (Laudon *et al.*, 1998), reducing the artifact to 20%. However, this is impractical for multichannel EEG recordings and the artifact reduction is far too small as EEG is typically 10–250 μV, whereas imaging artifact during fMRI can be many millivolts.

Felblinger described a method for eliminating the artifact induced by gradient fields, which appears to be effective for ECG recordings with gradient slew rates of 10 T m^{-1} s^{-1} (Felblinger *et al.*, 1999). This method determines the impulse response of the ECG recording system for gradient fields applied individually in the *x*, *y*, and *z* planes during a period of low-amplitude ECG (the ventricular diastole) with the assumption that the signals recorded were entirely induced artifact. These responses were then used to filter the *x*, *y*, and *z* gradient waveforms derived from the scanner during imaging and the sum of the filter outputs subtracted from the ECG. However, no quantitative results were given and the extension of this method to EEG signals recorded during fMRI may be inappropriate as the gradient slew rates in fMRI are an order of magnitude higher (typically 125 T m^{-1} s^{-1}) and EEG signals are an order of magnitude lower than ECG. In addition, there is no "quiet" period in the EEG signal during which the *x*, *y*, and *z* gradient artifacts can be measured. Although, as suggested, this could be overcome by averaging the responses over many epochs, the EEG of these must be uncorrelated and this would extend the time taken to perform this task. It is likely the process would need recalculating after even minor changes in the subject's position due to the high ratio of imaging artifact to EEG amplitude. In addition, we have observed that artifact sometimes persists after gradients have ceased changing. We speculate that this is due to small subject movements caused by scanner vibration during the gradient fields, taking a finite time to decay. As this artifact is induced by movement in the static field, it cannot be removed by modeling the effect of the gradient fields on the EEG.

Sijbers has reported a method for reducing imaging artifact by the subtraction from the EEG spectrum of a weighted average gradient artifact spectrum, followed by inverse Fourier transform (Sijbers *et al.*, 1999). This method was evaluated in EEG recorded from rats with gradient fields comparable to fMRI. Although this method increased the signal-to-artifact ratio by four to eight times, this is unlikely to be sufficient for EEG/fMRI in humans, for which the electrode loop areas, and hence induced artifact amplitude, are typically orders of magnitude larger.

Our preliminary assessment of image artifact waveforms recorded from subjects during periodic fMRI suggested that these artifact waveforms had very low intervolume variability and hence subtraction of the image artifact waveform averaged over a number of volume acquisitions might be effective (Josephs and Turner, 1998). This approach has been used successfully to remove pulse artifact from EEG/fMRI recordings (Allen *et al.*, 1998) and would avoid the complication of recording the impulse response for each gradient and could deal with artifact persisting after the cessation of gradients. For this method to be effective, the EEG recording system must have a large dynamic range to record both the EEG with appropriate resolution and the image artifact without saturation. We report here the design of an EEG recording system appropriate for recording of continuous EEG during event-related fMRI and a signal-processing based method for image artifact reduction (IAR) based on subtraction of averaged imaging artifact followed by adaptive noise cancellation.

METHODS

EEG Recording System

EEG is normally recorded with a resolution of ≤0.5 μV. However, for EEG/fMRI studies, which are nondiagnostic, a lower resolution of 2 μV is acceptable.

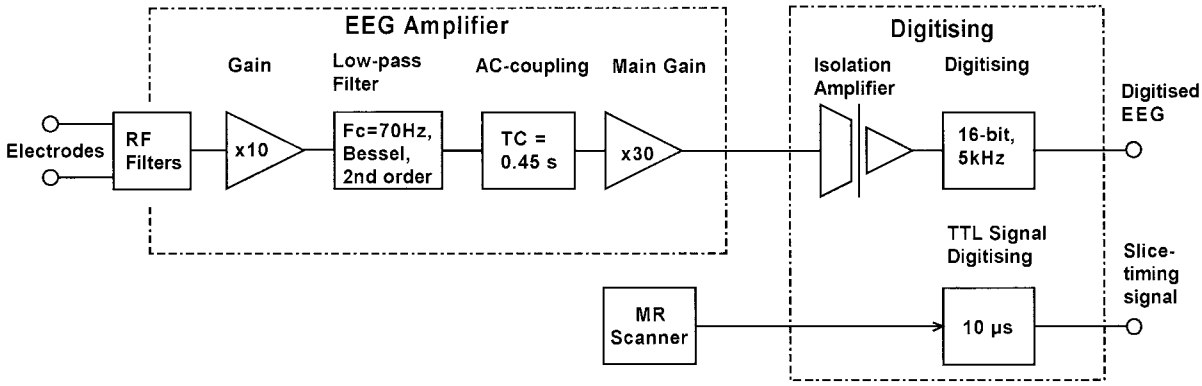

FIG. 1. Schematic of the EEG recording system.

Hence, if EEG is digitized using a 16-bit digitizer, which typically gives 14 bits in practice, the range of the EEG amplifier will be 33.3 mV peak to peak (pk-pk).

Artifacts are induced in the scalp and EEG leads by the changing magnetic fields applied during image acquisition (Faraday's law). Two different fields are applied: RF and gradients. Artifacts induced by RF have a much higher frequency than EEG and hence can be reduced effectively by low-pass filtering applied before the EEG amplifier front end. This is not the case for gradient artifact, which contains components in the EEG frequency range. The amplitude of induced gradient artifact is given by

$$V_{\mathrm{GAMax}} = (dB/dt)_{\max} \times A_{\max},$$

where V_{GAMax} is the maximum amplitude of induced gradient artifact, $(dB/dt)_{\max}$ is the maximum rate of change of gradient field, and $A_{\max}$ is the maximum loop area.

The maximum rate of change of gradient field is assumed to be 25 T s^{-1} (Siemens Vision 2T with a slew rate of 125 T m^{-1} s^{-1}, distance from the gradient coil isocenter assumed to be 0.2 m). The maximum loop area is assumed to be 100 cm^2, corresponding to widely spaced electrodes such as C4-A1 in the 10/20 system. This gives a maximum gradient artifact amplitude of 250 mV (500 mV pk-pk). This exceeds the EEG amplifier range defined above by a factor of 15 and will cause saturation.

Because much of this artifact is at frequencies above the EEG range, low-pass filtering can reduce it. We measured the maximum gradient artifact after low-pass filtering (second-order Bessel filter, 3-dB cut-off point of 70 Hz) for the slew rate and coil area described above, with the coil placed at the edge of the head-coil successively in the *x*, *y*, and *z* planes. This was ≈25 mV pk-pk, which is within the required range. Hence, an EEG amplifier was designed as follows (see also Fig. 1).

The electrode leads were connected to the amplifier via in-line filters designed to limit cable borne RF interference, with an attenuation of 70 dB at 85 MHz (the RF frequency for a 2-T scanner). The front end comprised an instrumentation amplifier with gain 10, which is small enough to prevent the image artifact waveforms saturating but helps to reduce the effects of noise introduced by subsequent stages. The next stage was a second-order Bessel low-pass filter (cut-off 70 Hz), which attenuates components above the scalp EEG frequency range (Ebner *et al.*, 1999). The EEG signal contains little of value above 50 Hz (Reilly, 1999). This filter was used as it has optimal phase linearity and thus a good transient response to the fast pulses in the image artifact waveform. The next stage applied AC coupling (time constant 0.33 s) to reduce DC potentials from the electrodes, before the main gain stage that set the overall gain to 300. Note that low-pass filtering was applied prior to the main gain stage so that the large-amplitude rapidly changing artifact waveforms were attenuated prior to significant gain, reducing the likelihood of saturation.

Signals were then passed from this EEG amplifier located in the scanner room, through a screened cable to an isolated amplifier (for safety) with gain of 1, bandwidth of DC to 1 kHz (CED1902; Cambridge Electronic Design, Cambridge UK), and then to a 16-bit digitizer (CED1401 Plus). Digitizer resolution at 14-bit level was 0.61 mV, corresponding to an EEG resolution of 2 μV and range of 33.3 mV as required. In this study we were not concerned with image quality and hence RF interference passed into the scanner room by the screened cable was not important.

EEG signals were recorded using Spike2 software (Cambridge Electronic Design) with a sample rate of 5 kHz per channel. A fMRI slice-timing signal, which defines accurately the time at the start of each slice and is sourced from the scanner, was captured with resolution of 10 μs and was used by the IAR algorithm to synchronize artifact averaging. A slice-timing signal

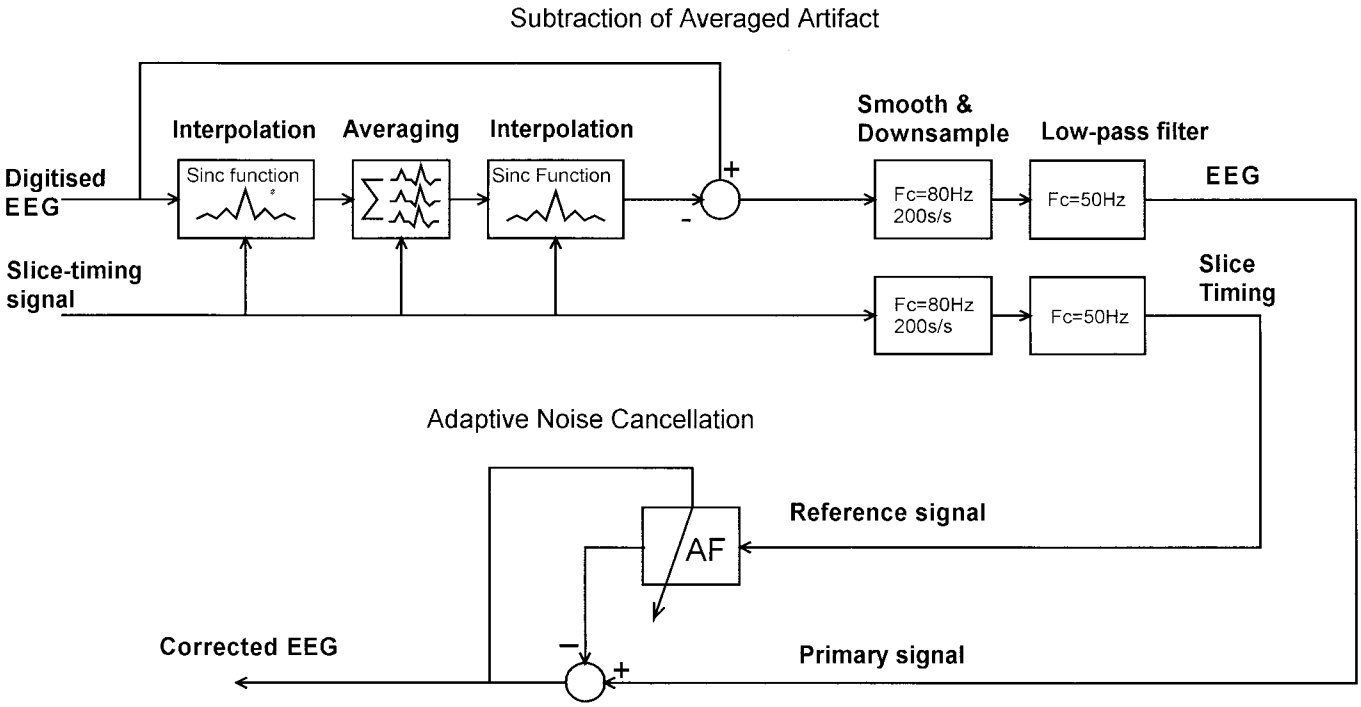

FIG. 2. Schematic of the IAR algorithm.

is commonly available from MR scanners hence this requirement does not restrict the general utility of the method.

Image Artifact Reduction

There are two stages to the IAR method. First, an average imaging artifact waveform is calculated over a fixed number of epochs and is then subtracted from the EEG for each epoch. Adaptive noise canceling is then used to attenuate any residual artifact (Fig. 2).

For a periodic fMRI sequence with delays between volume scans, an epoch was defined as the volume repeat time, TR. The EEG recording was divided into sections of 25 epochs over which averaging was performed. The rationale for selecting 25 epochs was that most EEG events are in the range 10–250 μV, and hence a minimum of 25 epochs must be averaged so that the largest likely EEG event is reduced below that of the smallest. This assumes that EEG is uncorrelated between epochs, which is likely as each volume scan normally lasts at least a few seconds. The artifact-to-EEG ratio is very high and hence 25 epochs is sufficient to obtain an accurate average. By dividing the EEG into fixed-length sections, the averaged artifact can adapt discretely throughout a recording.

For continuous fMRI acquisition, i.e., no delays between volumes, an epoch was defined as one slice. As the duration of a slice is typically less than 100 ms, correlation of EEG between successive epochs is likely. We assumed that EEG is uncorrelated over 0.3 s and for the purposes of artifact averaging divided the EEG into sections of 25×0.3 s $= 7.5$ s. For the continuous fMRI sequence used here, this corresponded to 7.5×13 slices/s $= 100$ slices.

For periodic fMRI, the averaging epoch included a period when no changing fields were applied. This was necessary as artifact was often observed to occur after the changing fields had ceased. This postimaging artifact had two components: an exponential part with a time constant equal to that for the AC coupling in the EEG amplifier (Fig. 5B) and a low-frequency decaying oscillation, possibly due to subject movement in the static field, caused by small scanner movements during application of the gradient fields.

When calculating the average artifact, the first five epochs in each section were always included—subsequent epochs were included only if the cross correlation function between the epoch and the current average exceeded 0.975. Although not optimal this scheme was a computationally efficient method for reducing averaged artifact corruption by atypical epoch signals, for example, those in which a subject movement occurred.

Imaging artifact is nearly perfectly synchronized to the slice-timing signal. To optimize calculation of the average artifact we used a 25-coefficient sinc function to interpolate the EEG values synchronous with the slice-timing signal. When subtracting the averaged artifact from the EEG in each epoch, a similar interpolation was performed in the reverse direction to synchronize the averaged waveform to the EEG samples.

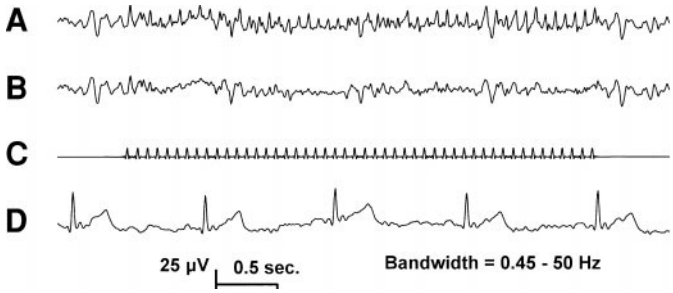

FIG. 3. The effect of adaptive noise cancellation. Trace A is signal Fp2-F4 after imaging artifact subtraction. Residual artifact at the slice frequency (12.4 Hz) is clearly visible and of amplitude approximately 30–50 μV. Trace B is the same signal after ANC. Trace C is the reference signal used by the ANC method and has been derived digitally by low-pass filtering of the slice-timing signals. Trace D is the ECG channel from the same recording and is shown here to confirm that the periodic peaks in trace B are pulse artifact rather than an error of the subtraction method.

After subtracting the average artifact, the signals were smoothed (eighth-order Chebyshev low-pass filter, cut-off 80 Hz applied in forward and reverse directions to give zero phase distortion) to reduce the likelihood of aliasing in the next process, which was downsampling to 200 Hz, a sampling rate typically used for EEG. Additional low-pass filtering was then performed (55 coefficient, finite impulse response, cut-off 50 Hz). Although subtracting the averaged artifact followed by low-pass filtering removed most of the artifact, some residual artifact, synchronized to the slice-timing signals, was sometimes observed (Fig. 3). For the sequences used, this resulted in 12.4- or 13.2-Hz signals, which clearly cannot be removed by linear filtering without affecting an important part of the EEG spectra. Adaptive noise canceling can reduce signal components correlated with a reference signal and was considered appropriate for removing this residual artifact.

We implemented an ANC filter similar to that described by Chen *et al.* (1989) as follows. The EEG signal with averaged artifact subtracted was used as the primary input. The reference signal applied to the tapped delay line adaptive filter was generated digitally for a sample rate of 200 Hz with value 0 for all samples except those when slice-timing signals occurred, which had value 1. This signal was then filtered using the 55-coefficient low-pass filter used to filter the EEG signals (Fig. 3, trace C).

The adaptive filter weights ($N = 20$) were adapted for every input sample using the Widrow–Hoff least mean squares algorithm to minimize the error between the filter output and the primary signal (Widrow *et al.*, 1975). The step size, which controls stability and convergence rate (normally referred to as μ), was set to 0.05/(number of weights $\times$ variance of the reference signal) (Chan *et al.*, 1995). The ANC filter was applied only to the EEG coincident with imaging, as residual artifact was present only during these periods. To reduce the discontinuity between these periods, the reference signal was tapered (raised cosine function) over the first and last 0.5 s of each period. The EEG output was taken as the difference between the primary signal and the adaptive filter output, that is, the EEG signal minus components correlated with the reference signal (Fig. 2). The algorithm was implemented using MATLAB V5.3 (The Mathworks, MA) and was applied offline.

Recordings

This study had the approval of the local ethical committee of The National Hospital for Neurology and Neurosurgery and all subjects gave written informed consent. EEG was recorded from five subjects (four male, one female, median age 35 years) in a Siemens 2T Vision scanner. In all five subjects, recordings were made during periodic fMRI (48-slice gradient echo EPI, 833 Hz, 20 mT/m sinusoidal readout, slice TR = 0.08 s, volume TR = 6 s). Additional recordings were made in two of these subjects using a continuous fMRI sequence (no gaps between successive volumes).

Recordings were made from adjacent electrodes in the 10–20 system at the following sites: O1–O2 (back of the head, *x* direction), Fz–Cz (top of the head, *y* direction), and Fp2–F4 (front of the head, *z* direction). Electrode spacing was 5.7 cm. In addition, electrodes C4–A1 were recorded to assess the method for the largest likely interelectrode lead loop (electrode spacing 20.5 cm). Gold electrodes were used, with a 15-kohm current-limiting resistor in each electrode lead to limit the maximum induced current (Lemieux *et al.*, 1997) and minimized interelectrode lead loops. The reference electrode was at Pz. Pulse artifact subtraction, which requires an ECG channel, is vital to interpret EEG/fMRI studies, hence an ECG channel was recorded from electrodes on the subject's back (via 75-kohm current-limiting resistors). The ECG channel provides confirmation that: (1) the method performs satisfactorily for electrodes farther from the magnet isocenter, where gradient-induced fields are stronger; (2) pulse artifact could be identified in the EEG after IAR; and (3) pulse artifact subtraction is effective for EEG after IAR. Electrode leads were brought out to the amplifiers at the front of the scanner via multicore cables.

The following periods were recorded, all with the subject's eyes closed. First, 2 min outside the scanner, to determine each subject's α frequency. Second, 2 min inside the scanner with no imaging to give a baseline to assess the IAR method. Third, EEG was recorded during fMRI: 10 min during periodic fMRI in all subjects, followed in two subjects by 3 min of continuous fMRI. In the middle of the fMRI, the subjects were asked to open and close their eyes periodically to give small subject movement and α suppression.

Validation

The median imaging artifact was measured for all channels, subjects, and recordings in the following data recorded during fMRI: (1) the raw EEG; (2) after down-sampling/low-pass filtering, but no IAR; (3) after subtraction of the averaged artifact and down-sampling/low-pass filtering; and (4) as in (3) but with ANC. The amplitude of imaging artifact was difficult to assess in stages (3) and (4) due to pulse artifact, hence we applied pulse artifact subtraction before making these measurements. In each case, the mean of 10 measurements, made at equally spaced intervals and always coinciding with fMRI, was calculated for each channel.

EEG signals recorded inside the scanner with no fMRI and with fMRI corrected by IAR were compared using spectral analysis. We did not compare the corrected EEG to that recorded outside the scanner, because the pulse artifact present only in the former makes this comparison meaningless. The average spectrum from 10 5.12-s periods (i.e., 1024 samples per period) equally spaced throughout the EEG recording was calculated for each channel and subject. Sections of EEG with eyes opened or obvious low-frequency artifacts (for example, those associated with small head movements) were excluded. The EEG recorded inside the scanner with no fMRI was down-sampled and low-pass filtered in exactly the same way as was used for IAR. The mean activity in four frequency bands (0.8–4, 4–8, 8–12, and 12–24 Hz) was then calculated for each EEG channel. The absolute value of percentage difference was then calculated for each channel as

$$\text{Percentage Difference} = 100 \times \text{absolute}\left((A_{\text{NI}} - A_{\text{IAR}})/A_{\text{NI}}\right),$$

where A_{NI} is the activity with no fMRI and A_{IAR} is the activity with fMRI corrected by IAR. The percentage differences for all channels and subjects were nonnormal, hence the median difference was calculated as a summary statistic.

To measure the ability of a reviewer to identify events in the EEG after artifact subtraction, epileptiform spike-wave complexes recorded from a subject with temporal lobe epilepsy (mean peak-to-peak amplitude 73.8 μV, SD 36.7 μV) were added digitally at random times to the raw EEG signals recorded during fMRI, giving a rate of one spike per 20 s of recording. We used spike-wave complexes as these contain both high- and low-frequency components. Spikes were added to the raw EEG data prior to IAR. Prior to review of these recordings, pulse artifact subtraction (Allen *et al.*, 1998) was applied to the corrected EEG. Two reviewers examined these recordings before and after artifact subtraction and the proportion of spike-waves correctly identified was calculated.

The presence of α rhythm in EEG outside the scanner and in the corrected EEG was also assessed. The criteria for identifying α in the corrected EEG were that the frequency and channels were the same as were recorded outside the scanner and that the frequency was less than the slice frequency (12.4 or 13.2 Hz).

RESULTS

Considering all recordings from all subjects, satisfactory recordings were obtained for 16 of the 20 EEG channels recorded. Four channels were excluded from further consideration due to large low-frequency artifacts (3 channels) and a failed electrode (1 channel). For the remainder, the maximum imaging artifact in the raw EEG was +9.16 mV, which is well within the range of the EEG recording system (±16.6 mV). For ECG the maximum was +16.3 mV, which is close to saturation. Clearly a lower gain channel for ECG would be advisable. The median value of imaging artifact in the raw EEG data was 4.0 mV pk-pk (range 0.6 to 17.3 mV). After down-sampling and low-pass filtering the median value decreased to 571 μV pk-pk (range 114 to 2890 μV), confirming that low-pass filtering alone cannot remove imaging artifact. The median artifact in each channel after subtraction of the average artifact (but prior to ANC) was 11 μV pk-pk (range 0 to 50 μV). ANC decreased this further to 8 μV pk-pk (range 0 to 28 μV). Hence, overall, a 500-fold reduction in imaging artifact was achieved. An example of the effectiveness of the IAR method and the shape of the averaged imaging and pulse artifact waveforms are shown in Fig. 4. Figure 5 shows the effect of artifact subtraction for a multichannel recording containing an added spike. For the spectral analysis, the median difference between EEG recorded inside the scanner with no fMRI and with fMRI followed by IAR was as follows: frequency band 0.8–4 Hz 10%, 4–8 Hz 10%, 8–12 Hz 14%, and 12–24 Hz 18%. The median number of spikes correctly identified in the recordings inside the scanner with fMRI was 12% (range 0 to 32%). This increased after IAR to 99% (70 to 100%), with only one false detection. α was clearly present in 4/5 subjects outside the scanner. α appeared to be present in 3/5 subjects in the scanner prior to imaging and in the same 3/5 in the corrected EEG.

DISCUSSION

The results from the recordings presented here confirm that imaging artifact is a significant problem in EEG recordings during fMRI. We measured a median artifact amplitude of 4000 μV pk-pk, which is over 400 times larger than the lowest amplitude EEG events and emphasizes the exactness required of the IAR method. Low-pass filtering reduced this to 571 μV, indicating that low-pass filtering alone is not sufficient

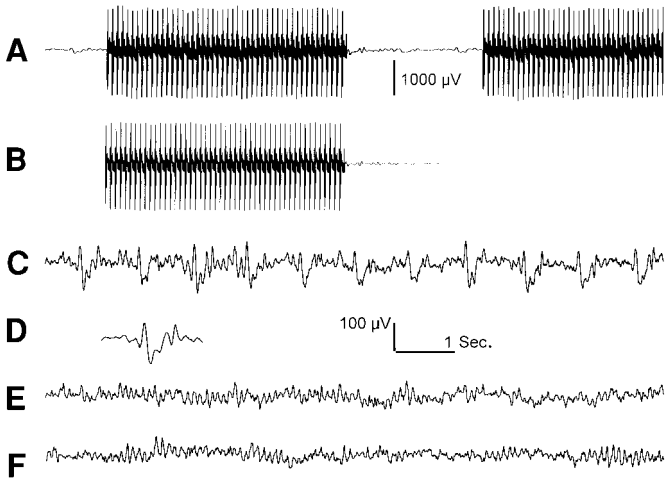

FIG. 4. The EEG waveforms (C4–A1) before and after imaging and pulse artifact subtraction. Bandwidth was 0.45 to 50 Hz. (A) The raw EEG during periodic fMRI. Large artifact is apparent during the 4 s of imaging (one volume), completely obscuring the EEG. The EEG during the 2-s gap between volume acquisitions appears to be relatively free of imaging artifact. (B) The averaged imaging artifact. Note that toward the end the EEG is almost flat, indicating that gradient-induced patient vibration persisting after the end of the volume acquisition has decayed and sufficient epochs have been averaged to attenuate cerebrally generated EEG. (C) The result of subtracting the averaged imaging artifact in B from the EEG in A, followed by down-sampling and ANC. Pulse artifact is now clearly present and imaging artifact is difficult to discern. The display scale has been increased from that in A and B. (D) The averaged pulse artifact from trace C (not to scale). (E) Result of subtracting the averaged pulse artifact in D from the EEG in C. A 10.5-Hz signal is apparent in this trace and this frequency matches that of this subject's α rhythm. (F) The EEG from the same subject, recorded *outside* the scanner, i.e., free of imaging and pulse artifact. The character of this EEG appears to match closely the artifact corrected trace in E.

to remove imaging artifact. Subtraction of the averaged artifact followed by low-pass filtering reduced this to 11 μV and ANC, the final stage of the IAR method, reduced this to 8 μV, indicating that the subtraction performs the bulk of the artifact subtraction and ANC suppresses the small amount of residual artifact. Epileptiform spike waves of lower amplitude than is commonly observed in temporal lobe epilepsy were almost totally obscured by the imaging artifact but were easily recognizable after applying the method. To ensure that the location of the spikes was known precisely they were added digitally to the raw EEG recorded during fMRI. This meant that the spikes were not recorded via the amplifiers and it is possible that the effect of amplifier saturation was thus not tested. However, the maximum imaging artifact magnitude recorded was only 55% of the amplifier range so saturation was unlikely to have occurred, and pulse artifact was clearly visible in all recordings, again indicating that amplifier saturation did not occur. α rhythm appeared to be present in 3/5 subjects in the corrected EEG although it was difficult to be certain as pulse artifact is known to contain strong components in the α frequency range (Allen *et al.,* 1998). Indeed, α was only detected in the same three subjects inside the scanner with no fMRI. Moreover, only small differences (10–18%) in spectral activity in four EEG frequency bands between corrected EEG and EEG recorded without fMRI were detected. Taken together, these measures indicate that the method removed a large proportion of the artifact and that EEG signal distortion was minimal.

The recording system reported here had sufficient dynamic range to record linearly both the background EEG activity of normal subjects and the high-amplitude imaging artifact, allowing digital signal-processing techniques to be used to reduce the artifact to acceptable levels. An important aspect of the amplifier design was the application of low-pass filtering prior to the main gain stage. This ensured that the large-amplitude high-frequency components of the imaging artifact were attenuated prior to large amplification, thus reducing the likelihood of saturation. In contrast, most electrophysiology amplifiers amplify and then filter, to minimize the effects of electrical noise introduced by the filters. Although RF filtering was applied at the front end of the EEG recording system, the waveforms recorded during imaging sometimes had a slowly changing baseline (for example in Fig. 5B). One possible explanation for this is that RF penetrated the front-end amplifier and was then demodulated to a low-frequency signal (the amplifier used for these recordings was a prototype and was not fully shielded). We are currently building shielded EEG amplifiers, which will transmit signals out of the scanner room via fiber optics. Nevertheless, we have demonstrated that despite RF breakthrough, low-noise EEG recordings are still possible.

For periodic fMRI, averaging by volume, as opposed to averaging by slice, was necessary for effective artifact removal, as the artifact waveform at the starting and stopping of fMRI differed from that of slices in-between, and decaying oscillations were sometimes observed after gradients ceased. We speculate that the altered waveforms at the start and stop of fMRI resulted from subject movement caused by scanner vibration due to the gradient fields, together with the effect of low- and high-pass EEG filters on the unbalanced imaging artifact signal. These filters are essential for anti-aliasing and electrode DC potential removal, respectively. It might be possible to remove some of this artifact by subtracting at the front-end the signal from an interference reference loop. However, as mentioned previously, Laudon found this technique reduced the artifact only to 20% for a single-channel ECG recording, for which the reference loop could be aligned optimally with the conductive tissue loop formed between electrodes (Laudon *et al.,* 1998). For multichannel EEG this approach is likely to perform

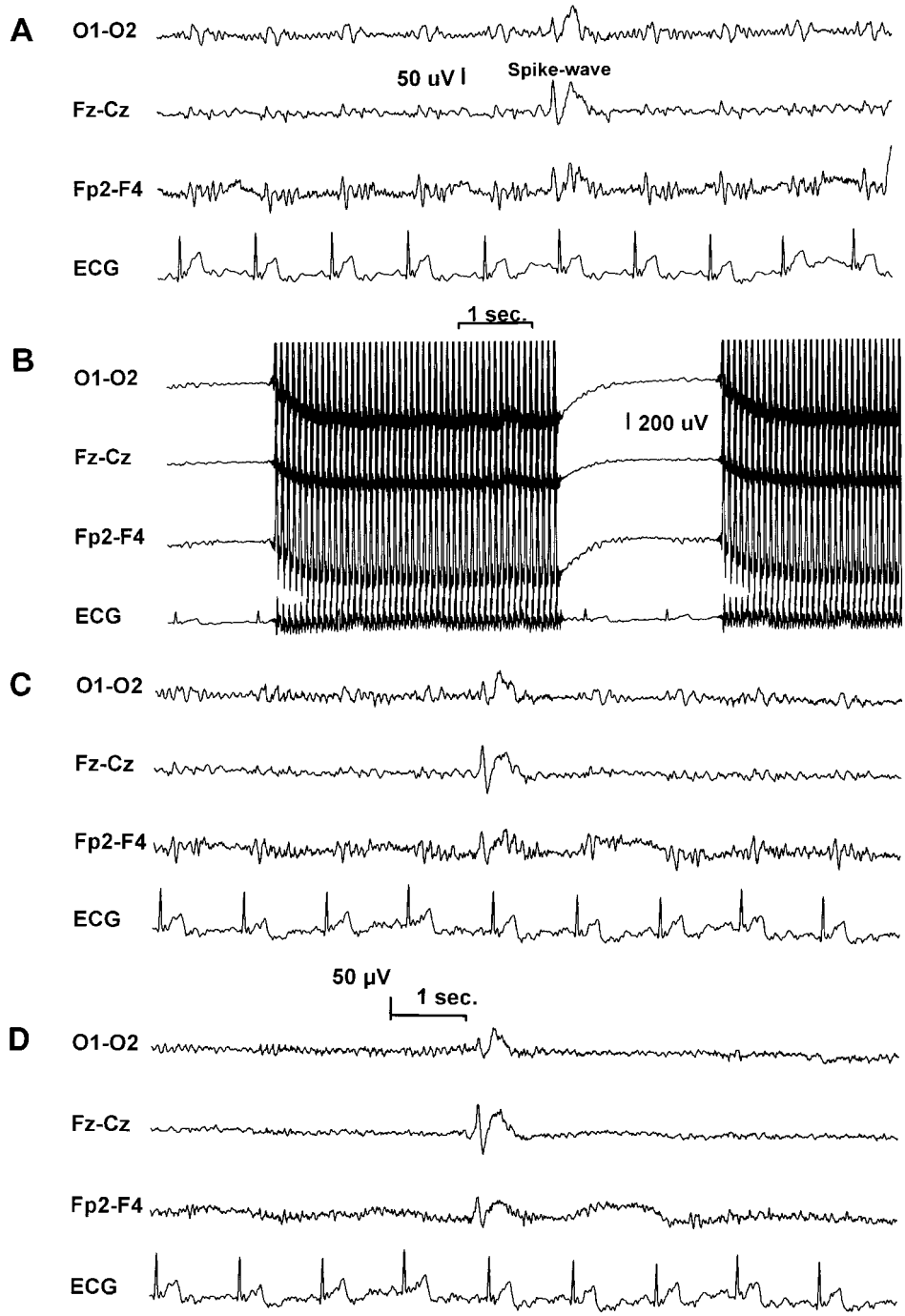

FIG. 5. The EEG signals recorded inside the scanner. In this subject, electrode C4 failed so C4–A1 is not shown. The ECG channel is scaled down four times lower than for the EEG plots. Bandwidth was 0.45 to 50 Hz. (A) These EEG signals were recorded in the absence of fMRI. A spike-wave complex added to the EEG is clearly visible, as is pulse artifact in the EEG channels (20–90 μV), synchronized to the ECG. These waveforms show the character of the EEG recorded inside the scanner, without fMRI and imaging artifact subtraction. (B) The uncorrected EEG signals (low-pass filtered and down-sampled) from the same subject during periodic fMRI. Because of the large amplitude of the artifact, all the channels have been scaled down four times compared to plots A, C, and D. The large amplitude of the imaging artifact, relative to the EEG, is clearly apparent. A spike-wave complex identical to that in plot A has been added to the EEG, prior to IAR. This is completely obscured by the imaging artifact. (C) The effect of the IAR method on the EEG signals shown in plot B. The spike wave is now clearly apparent and pulse artifact synchronized to the ECG channel is also clearly visible, indicating that no significant distortion of the EEG has occurred. (D) Pulse artifact subtraction has now been applied to the EEG signals in plot C and this has removed the pulse artifact almost entirely. This shows that in this case pulse artifact subtraction, which is vital for the interpretation of EEG recorded inside the MR scanner, can be applied effectively to signals corrected by the IAR method.

less well due to difficulties in aligning reference loops and would increase the complexity of electrodes or electrode application considerably. In view of the low residual noise relative to normal EEG achieved without this approach, it is probably not warranted for continuous EEG recording, although for lower amplitude event-related potentials (ERPs), it might possibly be justified.

Although subtraction of averaged artifact removed a large proportion of the imaging artifact, residual artifact was sometimes present. There are two causes of this: (1) jitter between the EEG sampling and scanner time frames and (2) differences between individual epochs and the average artifact, due to small subject movements. The former can be compensated for by interpolation, providing the imaging artifact is not aliased. To reduce aliasing while providing a good transient response, we used a second-order low-pass filter prior to digitizing at 5 kHz. Attenuation of this filter at the Nyquist point was 60 dB. A higher order analog filter might allow a lower sampling rate but these filters have poor transient responses and are not normally used in EEG recording systems as they distort EEG transients such as spikes (Ebner *et al.*, 1999)—they are clearly undesirable for accurate recording of the fast pulses present in imaging artifact.

We implemented interpolation using a 25-coefficient sinc function and recorded the slice-timing signal with a high temporal resolution (10 μs). A sinc function provides optimal interpolation for a band-limited signal. The sinc function coefficients are calculated for the required interpolation interval and are convolved with EEG to give the interpolated value. Although this requires considerably more calculation than simpler linear or quadratic polynomials interpolation, it was used to reduce the likelihood that residual artifact was due to interpolation errors. Although we have not investigated in detail the relationship between residual artifact and the interpolation method, preliminary testing suggests that if no interpolation was performed, i.e., the slice timing signal had the same temporal resolution as for the EEG (5 kHz), there was a clearly discernible increase in residual artifact prior to ANC but only a slight increase after ANC. Again, if a small increase in artifact can be tolerated, interpolation could be omitted, simplifying the implementation. The second source of error, differences between individual epochs and the average artifact, might be reduced by using a moving window average, particularly for continuous fMRI in which a short (7.5-s) averaging period was used. This would be less helpful for periodic fMRI with an averaging period of 150 s (25 × 6 s). Residual artifact resulting from both these sources of error is synchronized to the slice-timing signal and appeared to be reduced effectively by ANC.

Two different generic types of fMRI sequences were evaluated, namely continuous and periodic. For continuous acquisition, typical parameters were used and it is unlikely that adjustment of the main parameters (e.g., TE) would give poorer results. For periodic fMRI we noted that it was important to include in the averaging epoch the period several seconds after the cessation of changing fields, in which artifact was sometimes present. For the periodic fMRI sequence used in this work, the averaging epoch was set to the volume repeat time. For a sequence with a longer delay between volume scans, it would probably not be necessary to use the entire volume repeat time, and this would save computation. The method was validated for a 2-T scanner. The gradients for higher field strength scanners are not necessarily higher. The artifact caused by subject movement synchronized to the gradient fields would, however, increase linearly with field strength. As this component of the artifact was small compared to that induced directly by the gradient fields, this is unlikely to increase the residual artifact significantly.

In this work, the calculation and subtraction of averaged artifact were performed at a sampling rate of 5 kHz, and the resulting EEG was then smoothed and down-sampled to 200 Hz. The amount of computation could be reduced by smoothing and down-sampling prior to averaging. We observed a small increase in residual artifact associated with this approach, presumably due to an increase in interpolation errors.

The method was implemented offline. The averaging period for periodic fMRI was sufficiently long (25 × 6 s) to make an online implementation difficult. If the averaging epoch was set to one slice as opposed to one volume, unacceptably large artifact was observed, due to artifact variability occurring at the start and end of each volume scan. For continuous fMRI, however, the short averaging period used (7.5 s) would allow an online implementation.

The method has been evaluated for continuous EEG recordings during fMRI. Imaging artifact also affects the recording of ERPs during fMRI and the applicability of the IAR method to these recordings is of interest. Using a 16-bit digitizer, we were able to capture the worst case artifact without amplifier saturation, while measuring EEG with resolution of 2 μV. For ERPs, which are lower amplitude than EEG (typically 1–5 μV), greater dynamic range would be required. This could be achieved by using a higher resolution digitizer. Although the residual noise after IAR was several times greater than typical ERP signal levels, this does not preclude ERP recording, as imaging artifact is uncorrelated with the ERP and hence can be attenuated further by averaging, an approach that is not possible for continuous EEG. The 70-Hz low-pass filter in the front end was not inappropriate for cognitive ERPs (low pass typically 30–100 Hz), which is the ERP of most relevance for fMRI studies. For VEPs (low pass 250 Hz) and certainly SEPs (low pass 2000 Hz) a higher cut-off would be desirable. A higher cut-off

would have two consequences: frequency components in the imaging artifact signal above the Nyquist point (2.5 kHz) would be larger giving aliasing, and lower frequency components in the imaging artifact, in the ERP range, would also be increased giving greater residual artifact. The former problem could be overcome by increasing the sampling rate, the latter may require more sweeps.

CONCLUSION

In EEG/fMRI studies, large-amplitude artifacts induced in the EEG by the changing fields applied during image acquisition normally obscure the EEG completely, limiting study design. We have developed a signal-processing based method, which uses subtraction of an averaged artifact waveform followed by adaptive noise cancellation to reduce this artifact effectively. This method was validated in recordings from five subjects using two fMRI sequences by measurement of residual artifact, spectral analysis, and identification of spike-wave complexes in the corrected EEG. The amplitude of residual imaging artifact after IAR was below 10 μV, whereas EEG signals are typically 10–250 μV, indicating acceptable level of artifact reduction. Spectral differences of only 10–18% between corrected EEG and EEG with no fMRI were found and over 99% of spike waves were identified in the corrected, compared to 12% in the uncorrected, EEG. α rhythm was identified in 3/5 subjects in the corrected EEG. All these measures indicate that a high proportion of the artifact was removed and minimal EEG distortion occurred. Careful design of the EEG amplifier was essential to provide sufficient dynamic range to capture both low-amplitude EEG and the large artifact without distortion to enable this signal-processing based method to be effective. Using the recording apparatus and artifact reduction method described in this paper, we have demonstrated that simultaneous EEG and fMRI recording is for the first time possible, extending the scope of combined EEG/fMRI studies considerably.

ACKNOWLEDGMENT

The authors acknowledge the support of Dr. Louis Lemieux at the National Society for Epilepsy, Chalfont St. Peter, Buckinghamshire, UK.

REFERENCES

Allen, P. J., Polizzi, G., Krakow, K., Fish, D. R., and Lemieux, L. 1998. Identification of EEG events in the MR scanner: The problem of pulse artifact and a method for its subtraction. *NeuroImage* **8:** 229–239.

Chan, F. H. Y., Lam, F. K., Poon, P. W. F., and Qiu, W. 1995. Detection of brainstem auditory evoked potential by adaptive filtering. *Med. Biol. Eng. Comput.* **33:** 69–75.

Chen, J., Vandewalle, J., Sansen, W., Vantrappen, G., and Janssens, J. 1989. Adaptive method for cancellation of respiratory artifact in electrogastric measurements. *Med. Biol. Eng. Comput.* **27:** 57–63.

Ebner, A., Sciarretta, G., Epstein, C. M., and Nuwer, M. 1999. EEG Instrumentation. In *Recommendations for the Practice of Clinical Neurophysiology: Guidelines of the International Federation of Clinical Neurophysiology* (G. Deuschl and A. Eisen, Eds.). *Electroencephalogr. Clin. Neurophysiol. Suppl.* **52:** 7–10.

Felblinger, J., Slotboom, J., Kreis, R., Jung, B., and Boesch, C. 1999. Restoration of electrophysiological signals distorted by inductive effects of magnetic field gradients during MR sequences. *Magn. Reson. Med.* **41:** 715–721.

Hill, R. A., Chiappa, K. H., Huang-Hellinger, F., and Jenkins, B. G. 1995. EEG during MR imaging: Differentiation of movement artifact from paroxysmal cortical activity. *Neurology* **45:** 1942–1943.

Huang-Hellinger, F., Breiter, H. C., McCormack, G., Cohen, M. S., Kwong, K. K., Sutton, J. P., Savoy, R. L., Weisskoff, R. M., Davis, T. L., Baker, J. R., Belliveau, J. W., and Rosen, B. R. 1995. Simultaneous functional magnetic resonance imaging and electrophysiological recording. *Hum. Brain Mapp.* **3:** 13–23.

Josephs, O., Turner, R., and Friston, K. 1997. Event related fMRI. *Hum. Brain Mapp.* **5:** 243–248.

Josephs, O., and Turner, R. 1998. An adaptive MRI gradient noise filter. *NeuroImage* **7:** S590.

Krakow, K., Woermann, F. G., Symms, M. R., Allen, P. J., Lemieux, L., Barker, G. B., Duncan, J. S., and Fish, D. R. 1999. EEG-triggered functional MRI of interictal epileptiform activity in patients with partial seizures. *Brain* **122:** 1679–1688.

Kreger, K. S., and Giordano, C. R. 1992. Biopotential adaptive filtering in an MR environment. In *Abstracts SMRM 11th Annual Scientific Meeting,* Vol. 1, p. 661.

Laudon, M. K., Webster, J. G., Frayne, R., and Grist, T. M. 1998. Minimizing interference from magnetic resonance imagers during electrocardiography. *IEEE Trans. Biomed. Eng.* **45:** 160–163.

Lemieux, L., Allen, P. J., Franconi, F., Symms, M. R., and Fish, D. R. 1997. Recording of EEG during fMRI experiments: Patient safety. *Magn. Reson. Med.* **38:** 943–952.

Patel, P., and Al-Dayeh Singh, M. 1997. Localisation of alpha activity by simultaneous fMRI and EEG measurements. *Proc. Int. Soc. Magn. Reson. Med.* **3:** 1653.

Portas, C. M., Krakow, K., Allen, P. J., Josephs, O., and Frith, C. 1999. Sensory processing across the sleep–wake cycle: A functional MRI study in humans. *Soc. Neurosci. Abstr.* **25:** 2065.

Reilly, E. L. 1999. EEG recording and operation of apparatus. In *Electroencephalography: Basic Principles, Clinical Applications and Related Fields,* 4th ed. (E. Niedermeyer and F. Lopes Da Silva, Eds.), pp. 122–142. Williams & Wilkins, Baltimore.

Seeck, M., Lazeyras, F., Michel, C. M., Blanke, O., Gericke, C. A., Ives, J., Delavelle, J., Golay, X., Haenggeli, C. A., de Tribolet, N., and Landis, T. 1998. Non-invasive epileptic focus localisation using EEG-triggered functional MRI and electromagnetic tomography. *Electroencephalogr. Clin. Neurophysiol.* **106:** 508–512.

Sijbers, J., Michiels, I., Verhoye, M., Van Auderkerke, J., Van der Linden, A., and Van Dyck, D. 1999. Restoration of MR-induced artifacts in simultaneously recorded MR/EEG data. *Magn. Reson. Imag.* **17:** 1383–1391.

Warach, S., Ives, J. R., Schlaug, G., Patel, M. D., Darby, D. G., Thangaraj, V., Edelman, R. R., and Schomer, D. L. 1996. EEG-triggered echo-planar functional MRI in epilepsy. *Neurology* **47:** 89–93.

Widrow, B., Glover, J. R., McCool, J. M., Kaunitz, J., Williams, C. S., Hearn, R. H., Zeidler, J. R., Dong, E. F. J., Jr., and Goodlin, R. C. 1975. Adaptive noise cancellation: Principles and applications. *Proc. IEEE* **63:** 1692–1716.